DR. SHILONG PIAO (Orcid ID : 0000-0001-8057-2292)

Article type : Primary Research Articles

Attribution of seasonal leaf area index trends in the northern latitudes with "optimally" integrated ecosystem models

Running head: Attribution of seasonal LAI trends

Zaichun Zhu [1], Shilong Piao [1,2*], Xu Lian [1], Ranga B. Myneni [3], Shushi Peng [1], Hui Yang[1]

[1] Sino-French Institute for Earth System Science, College of Urban and Environmental Sciences, Peking University, Beijing 100871, China.

[2] Key Laboratory of Alpine Ecology and Biodiversity, Institute of Tibetan Plateau Research, CAS Center for Excellence in Tibetan Plateau Earth Science, Chinese Academy of Sciences, Beijing 100085, China.

[3] Department of Earth and Environment, Boston University, Boston, Massachusetts 02215, USA.

* ***Corresponding author:*** *Dr. Shilong Piao,* Sino-French Institute for Earth System Science, College of Urban and Environmental Sciences, Peking University, Beijing 100871, China. Tel: 86-010-62753298, *Email: slpiao@pku.edu.cn*

Keywords: Attribution**,** vegetation greening, seasonal change, remote sensing, climate change, Bayesian model averaging

Paper Type: Primary research

Manuscript for *Global Change Biology*

Abstract

Significant increases in remotely sensed vegetation indices in the northern latitudes since the 1980s have been detected and attributed at annual and growing season scales. However, we presently lack a systematic understanding of how vegetation responds to asymmetric seasonal environmental changes. In this study, we first investigated trends in the seasonal mean leaf area index (LAI) at northern latitudes (north of 30°N) between 1982 and 2009 using three remotely sensed long-term LAI data sets. The most significant LAI increases occurred in summer (0.009 m^2 m^{-2} yr^{-1}, $p < 0.01$), followed by autumn (0.005 m^2 m^{-2} yr^{-1}, $p < 0.01$) and spring (0.003 m^2 m^{-2} yr^{-1}, $p < 0.01$). We then quantified the contribution of elevating atmospheric CO_2 concentration (eCO_2), climate change, nitrogen deposition, and land cover change to seasonal LAI increases based on factorial simulations from 10 state-of-the-art ecosystem models. Unlike previous studies that used multi-model ensemble mean (MME), we used the Bayesian model averaging (BMA) to optimize the integration of model ensemble. The optimally integrated ensemble LAI changes are significantly closer to the observed seasonal LAI changes than the traditional MME results. The BMA factorial simulations suggest that eCO$_2$ provides the greatest contribution to increasing LAI trends in all seasons (0.003–0.007 m^2 m^{-2} yr^{-1}), and is the main factor driving asymmetric seasonal LAI trends. Climate change controls the spatial pattern of seasonal LAI trends and dominates the increase in seasonal LAI in the northern high latitudes. The effects of nitrogen deposition and land use change are relatively small in all seasons (around 0.0002m^2 m^{-2} yr^{-1} and 0.0001–0.001 m^2 m^{-2} yr^{-1}, respectively). Our analysis of the seasonal LAI responses to the interactions between seasonal changes in environmental factors offers a new perspective on the response of global vegetation to environmental changes.

Introduction

In the context of rapid environmental changes, e.g., rising atmospheric CO$_2$ concentration, climate change, nitrogen deposition, and land use change, monitoring and analyzing vegetation dynamics have become a pivotal subject in global change research in recent decades (Donohue *et al.*, 2013, Keeling *et al.*, 1996a, Los, 2013, Lucht *et al.*, 2002, Mao *et al.*, 2016, Mao *et al.*, 2013, Myneni *et al.*, 1997, Piao *et al.*, 2015, Zhou *et al.*, 2001, Zhu *et al.*, 2016). A growing body of literature demonstrates that vegetation generally show “greening” trends at annual and/or growing season time scale during recent decades(Los, 2013, Mao *et al.*, 2016, Piao *et al.*, 2015, Xu *et al.*, 2013, Zhu *et al.*, 2016). However, the environment has been changing rapidly and with asymmetric seasonal trends in recent decades (IPCC, 2013), raising the question of how vegetation will respond. Long-term temperature observations reveal asymmetric seasonal temperature trends in the northern latitudes between 1979 and 2010, with significant warming trends in all seasons except winter (Cohen *et al.*, 2012). Changes in total precipitation in northern vegetated lands have not been significant in all seasons, but the spatial pattern of seasonal precipitation trends indicates substantial changes in local seasonal precipitation (Fig. S1 and S9). These asymmetric changes in seasonal climate conditions are expected to significantly alter seasonal vegetation growth, but this effect cannot be directly detected in studies based on annual analyses (Mao *et al.*, 2016, Piao *et al.*, 2011, Wang *et al.*, 2011b, Zhu *et al.*, 2016).

Studies revealed that some ecosystem processes have been responding to the seasonal climate change. For example, changes in spring and autumn climate have resulted in an extended growing season in the northern latitudes (Jeong *et al.*, 2011, Liu *et al.*, 2016, Piao *et al.*, 2007), which are supposed to contribute to increased vegetation growth due to a longer photosynthesis period. Increases in temperature and water stress during summer, however, appear to have caused higher tree mortality rates (Allen *et al.*, 2010, Hember *et al.*, 2017), resulting in a net decrease in vegetation growth. The effects on vegetation growth of seasonal changes in other environmental factors, as well as their interactions with seasonal climate change effects, are presently unclear (Anderegg *et al.*, 2015, Greaver *et al.*, 2016, Reich *et al.*, 2014, Sitch *et al.*, 2003). Specifically, the response of vegetation to eCO_2 concentration likely varies with seasonal changes in biotic and abiotic factors(Lewis *et al.*, 1996). For example, the extended growing season caused by climate change in the northern latitudes allows a longer time for eCO_2 effects to propagate; however, hydrothermal conditions during the extended growing season may not promote these effects. Thus, eCO_2 effects are predicted to be stronger during summer than in other seasons due to higher temperatures; however, continuous warming may hamper eCO_2 effects once the temperature exceeds the optimum for vegetation growth (Medlyn *et al.*, 2002). Additionally, temperature-induced water deficiency may limit eCO_2 effects on vegetation in summer (Chaves *et al.*, 2002), although eCO_2 typically increases water use efficiency in vegetation to some extent (Huang *et al.*, 2016, van der Sleen *et al.*, 2015). Detailed studies of the seasonal effects of environmental factors on vegetation and their interactions improve our understanding of vegetation dynamics and their driving factors, demonstrating the need for more effective approaches to detecting and analyzing seasonal vegetation changes.

Compared to previous statistical modeling methods(Los, 2013, Wu *et al.*, 2015, Zhou *et al.*, 2001), ecosystem process models are more effective in separating the contributions of environmental factors to changes in seasonal vegetation growth (Piao *et al.*, 2006b, Sitch *et al.*, 2003). When an ensemble of ecosystem model simulations with prescribed simulation protocol are available, the MME mean is a widely used approach to minimize uncertainties in model simulations. MME method inherently integrate the model ensemble by giving equal weight to each model regardless of its performance (Flato *et al.*, 2013, Le Quéré *et al.*, 2015, Martre *et al.*, 2015, Piao *et al.*, 2015, Zhu *et al.*, 2016). In contrast to this “one vote per model” method, another type of approach integrate the ensemble members based on model basis or model performance (Flato *et al.*, 2013). For example, the Bayesian model averaging

(BMA) method provides an optimal strategy for evaluating model performance and integrate model simulations (Hoeting *et al.*, 1999, Vrugt *et al.*, 2008). The "optimal" integrated ensembles typically perform better than MME mean or most of the individual models and has been widely used as optimal estimates for climate models (Flato *et al.*, 2013, Furrer *et al.*, 2007, Giorgi & Mearns, 2002, Milliff *et al.*, 2011, Tebaldi & Knutti, 2007). However, the "optimal" integration approaches received less attention in the ecosystem modelling communities.

The primary objective of this study was to quantify seasonal trends in vegetation growth, and to quantify the contributions of their potential driving factors, including eCO_2, climate change, nitrogen deposition, and land cover change. We used the mean monthly leaf area index (LAI) during three seasons (March–May, MAM; June–August, JJA; September–November, SON) as a proxy for seasonal vegetation growth. Three remotely sensed LAI products, i.e., Global Inventory Modeling and Mapping Studies (GIMMS) LAI3g (Zhu *et al.*, 2013), Global Land Surface Satellites (GLASS) LAI (Xiao *et al.*, 2014), and Global Mapping (GLOBMAP) LAI (Liu *et al.*, 2012), were used to quantify changes in seasonal LAI measurements and their uncertainties in the northern latitudes (north of 30°N). We also analyzed the relative contributions of each season to annual LAI increases between 1982 and 2009. To analyze the observed changes in seasonal LAI, we designed four experimental simulations (S1: varying CO_2 only; S2: varying CO_2 and climate; S3: varying CO_2, climate, and nitrogen deposition; S4: varying CO_2, climate, and land cover change) with 10 state-of-the-art ecosystem models (CLM4.5, LPJ, LPJ-GUESS, LPX-Bern, OCN, ORCHIDEE, VISIT, CLM4, CABLE, and VEGAS) (Le Quéré *et al.*, 2013, Sitch *et al.*, 2015). For comparison to the traditional MME mean method, we used a Bayesian model averaging (BMA) strategy to minimize model uncertainties by optimizing the integration of model simulations.

Materials and methods

Remotely sensed LAI data sets

Remote-sensing LAI provides an efficient way to continuously monitor global vegetation dynamics at high frequency. Remotely sensed LAI data have been widely used to detect changes in regional and global vegetation growth (Dardel *et al.*, 2014, Wu *et al.*, 2016, Xu *et al.*, 2013), and they can be linked to ecosystem models to investigate the contributions of potential drivers of vegetation changes (Mao *et al.*, 2016, Piao *et al.*, 2006a, Piao *et al.*, 2015, Zhu *et al.*, 2016). In this study, we applied three widely used long-term remotely sensed LAI products (GIMMS LAI3g, GLASS LAI, and GLOBMAP LAI) to quantify trends in seasonal LAI values and their uncertainties in the northern latitudes (north of 30°N).

GIMMS LAI3g. GIMMS LAI was derived from the third-generation Advanced Very High Resolution Radiometer (AVHRR) GIMMS Normalized Difference Vegetation Index (NDVI) data set and best-quality Moderate Resolution Imaging Spectroradiometer (MODIS) LAI using artificial neural network (ANN) models (Zhu *et al.*, 2013). The quality and research applicability of the GIMMS LAI3g dataset were evaluated through comparisons with field LAI measurements, inter-comparisons with other satellite data products, and statistical analyses with large-scale climatic variations. The GIMMS LAI3g dataset, which provides LAI observations at 15-day temporal resolution and 1/12 ° spatial resolution for global vegetation from July 1981 to December 2011, has been widely used for various research purposes (Anav *et al.*, 2013a, Bellucci *et al.*, 2015, Huang *et al.*, 2015, Mao *et al.*, 2016, Murray-Tortarolo *et al.*, 2013, Shen *et al.*, 2015, Sitch *et al.*, 2015, Yan *et al.*, 2013, Zhu *et al.*, 2016).

GLASS LAI. The GLASS LAI data set was derived from AVHRR, MODIS, and CYCLOPES reflectance and LAI products using general regression neural networks (Xiao *et al.*, 2014). The GLASS LAI provides global LAI products at 8-day temporal resolution and 1-km spatial resolution from 1981 to 2012 (http://www.bnu-datacenter.com/). Field measurements and validation of CYCLOPES and MODIS LAI products indicate that the GLASS LAI data set is appropriate for the study of long-term global vegetation dynamics.

GLOBMAP LAI. The GLOBMAP LAI product was generated by quantitative fusion of historical AVHRR (1981–2000) and MODIS (2000–2011) data (Liu *et al.*, 2012). The pixel-level relationship between AVHRR observations (GIMMS NDVI) (Tucker *et al.*, 2005) and MODIS LAI was first established for the overlapping period 2000–2006, and then used to estimate AVHRR LAI from historical AVHRR observations backward to 1981. The GLOBMAP LAI is a combination of the AVHRR and MODIS LAI, with global coverage at 15-day temporal resolution and 8-km spatial resolution for the period 1981–2011 (http://www.modis.cn/globalLAI/).

Process-based ecosystem models

We simulated gridded monthly LAI in the northern latitudes between 1982 and 2009 with 10 state-of-the-art ecosystem models. Seven of these models (CLM4.5, LPJ, LPJ-GUESS, LPX-Bern, OCN, ORCHIDEE, and VISIT) were coordinated by the “Trends and drivers of the regional scale sources and sinks of carbon dioxide” project phase 2 (TRENDYv2) (Le Quéré *et al.*, 2013, Sitch *et al.*, 2015). Three other models (CLM4, CABLE, and VEGAS) were run under protocols similar to those for the seven TRENDYv2 models (Lawrence *et al.*, 2011, Wang *et al.*, 2010, Zeng *et al.*, 2000). All models performed simulations S1 and S2 using global atmospheric CO_2 concentration (Keeling & Whorf,

2005) and historical climate fields from the Climatic Research Unit National Centers for Environmental Prediction (CRUNCEP) data set(New *et al.*, 2000). In simulation S1, models were forced with changing atmospheric CO_2 concentration, while climate was held constant. Both atmospheric CO_2 concentration and climate were varied in simulation S2. Two models (CLM4 and CABLE) performed simulation 3 (S3) with varying atmospheric CO_2 concentration, climate, and nitrogen deposition. The average differences between S3 and S2 of CLM4 and CABLE were used to assess the relative contribution of nitrogen deposition. The seven TRENDYv2 models performed simulation 4 (S4), in which CO_2 concentration, climate, and land cover were varied. The differences between S4 and S2 were used to evaluate the response of vegetation growth to land cover change. To further understand the response of vegetation to changes in individual climatic variables, we ran an additional set of simulations with the Organizing Carbon and Hydrology in Dynamic Ecosystems (ORCHIDEE) model: (C1) varying atmospheric CO_2 concentration, temperature, precipitation, and radiation; (C2) varying CO_2, precipitation, and radiation; (C3) varying CO_2, temperature, and radiation; and (C4) varying CO_2, temperature, and precipitation. We assessed the effects of temperature, precipitation, and radiation on vegetation growth by individually subtracting C2, C3, and C4 from C1. All model outputs and remotely sensed LAI data were composited to monthly temporal resolution and resampled to a common spatial resolution (0.5°) using the bicubic method.

Bayesian model averaging

We determined the optimal integration weights for the 10 ecosystem models according to their performance on simulating seasonal mean LAI anomalies using the Bayesian model averaging approach (Vrugt *et al.*, 2008). A suite of different simulation researches has demonstrated that the BMA method produces more reliable simulations than other available multi-model approaches (Ajami *et al.*, 2007, Neuman, 2003, Raftery *et al.*, 2005). The optimal probability density function (pdf) of seasonal LAI anomalies (L) is defined as $p(L|f_1,\dots,f_{10}) = \sum_{k=1}^{10} w_k\, g_k(L|f_k)$, where $f = f_1, f_2, \dots, f_{10}$ denote an ensemble of simulations obtained from the 10 ecosystem models, $g_k(L|f_k)$ represents the conditional pdf of L on f_k, and w_k denotes the posterior probability of simulation *k* being the best one. w_ks are estimated by Monte Carlo Markov chains based on the maximum likelihood function (Vrugt *et al.*, 2008). The seasonal mean LAI anomalies simulated by the 10 ecosystem models and observed seasonal mean LAI anomalies for the period 1982–2009 were aggregated for each 3×3 grid window before estimating the weights for the ecosystem models using the BMA method. The arithmetic sum of the weights of all models is equal to one, and models with higher weights are believed to perform better at the given grid window. We then calculated the BMA model ensemble by summing the weighted model simulations. The same weights were used to calculate ensembles of seasonal mean LAI anomalies for all factorial simulations.

We used linear least squares regression to estimate trends in the seasonal mean of satellite-observed monthly LAI and the seasonal mean of monthly LAI simulated by ecosystem models under predefined scenarios. Trends in seasonal LAI were compared using Student's t-test, and considered statistically significant at $p < 0.05$.

Results

Trends in seasonal LAI

Seasonal mean LAI in the northern latitudes increased significantly ($p < 0.05$) in all three growing seasons. The average trends in seasonal mean LAI were $0.003_{-0.002,GLOBMAP}^{0.008,GLASS}$ m^2 m^{-2} yr^{-1} ($p < 0.01$), $0.009_{0.005,GIMMS}^{0.015,GLASS}$ m^2 m^{-2} yr^{-1} ($p < 0.01$) and $0.005_{0.003,GLOBMAP}^{0.007,GLASS}$ m^2 m^{-2} yr^{-1} ($p < 0.01$) for MAM, JJA, and SON, respectively (Fig. 1a). Earlier onset of the growing season was more prominent than delayed end of season (EOS) in the northern hemisphere (Liu *et al.*, 2016); however, trends in LAI during SON were greater than those during MAM. The most substantial increases in LAI were observed during JJA; these were more than triple those in the onset (March and April) and dormancy months (October and November). These results indicate that the earlier start of season (SOS) in spring and delayed EOS are not likely to have been dominant driving factors for the greening trends.

More than half of the vegetated area showed significantly increasing ($p < 0.05$) trends in seasonal mean LAI during JJA ($60.8\%_{29.3\%,GLASS}^{67.7\%,GIMMS}$) and SON ($50.6\%_{28.8\%,GLASS}^{57.4\%,GIMMS}$), whereas approximately one third of the vegetated area showed significant increases ($p < 0.05$) in seasonal mean LAI during MAM ($35.1\%^{61.6\%,GIMMS}_{25.5\%,GLASS}$). The most notable greening regions were Europe, southeastern China, eastern North America, and Siberia (Fig. 1b, c, and d). Among these regions, Europe and southeastern China exhibited notable greening trends (>0.02 m^2 m^{-2} yr^{-1}) in all three seasons, whereas eastern Siberia showed notable greening trends in JJA. In contrast, decreasing trends were observed over less than 5% of the northern vegetated area during all three growing seasons. There were significant uncertainties among the three observed seasonal LAI trends. The spatial distributions of the range of grid-level LAI trends (defined as the difference between the maximum and minimum trends among the three trend values derived from the three remotely sensed LAI products) showed that the three observed LAI products displayed notable discrepancies in seasonal LAI trends, particularly during JJA (Fig. S3). Large differences (>0.012 m^2 m^{-2} yr^{-1}) were found, mainly in the mid–high latitudes and in eastern North America, Europe, eastern Siberia, and southeastern China. Most of the largest trends were derived from GLASS LAI for all three growing seasons, whereas the smallest trends for most regions were estimated from GLOBMAP LAI during MAM, and GIMMS LAI and GLOBMAP LAI during JJA and SON.

Fig. 2a shows the spatial pattern of the dominant greening/browning seasons, i.e., the seasons that made the greatest contribution to the annual increasing/decreasing trends. JJA was the dominant greening season over 62.3% of the northern vegetated lands, followed by SON (14.2%) and MAM (11.4%) (Fig. 2b). The regions where JJA dominated annual greening were distributed over most of the vegetated lands in Eurasia and over high latitudes in North America. JJA contributed more than 80% of the annual net greening trends in the northern high latitudes and northeast Asia, whereas its dominant role was less prominent in

Eastern Europe and at lower latitudes. The regions where MAM dominated the annual greening were mainly distributed in Western Europe and eastern and central Asia. The regions where SON dominated the annual greening area were discretely distributed within North America and Europe.

Browning occurred over a greater area during JJA and SON (45.8 and 29.8%, respectively). One region where JJA dominated the annual browning trends extended over northern China and eastern Mongolia, where water availability is limited (Nemani *et al.*, 2003). The decreases in LAI during JJA reached approximately 80% of the annual net LAI decreases. The regions where annual browning occurred mainly in SON were sparse, located in northeastern North America and some parts of northern Russia.

Attribution of seasonal trends in vegetation LAI

We evaluated the performance of the 10 state-of-the-art ecosystem models in simulating seasonal LAI in the northern latitudes using the Taylor diagram (Fig. 3). LAI simulated by individual models and MME mean LAI were compared to remotely sensed LAI for northern lands. The performance of the modeled LAI was quantified by correlation coefficients (R) between the modeled and observed LAI, standard deviation (SD) of the inter-annual variation in the seasonal LAI time series, and the root mean square difference (RMSD) between the modeled and observed LAI (Taylor, 2001). Generally, the model-simulated seasonal LAI values were comparable to the observed seasonal LAI. For the study area, correlation coefficients between model-simulated seasonal LAI and observed LAI ranged from

$0.695_{0.320,LPJ}^{0.712,CLM4}$ (mean_{min}^{max}) for SON to $0.873_{0.620,OCN}^{0.876,VISIT}$ for JJA. SD and RMSD values between the modeled and observed LAI also suggest overall acceptable performance by the ecosystem models in reproducing observed northern latitudinal seasonal LAI variation (SD ranging from 0.041 m^2m^{-2} for MAM to 0.075 m^2m^{-2} for JJA) in the northern latitudes (SD ranging from $0.054_{0.035,CABLE}^{0.126,VISIT}$ m^2m^{-2} for MAM to $0.066_{0.034,ORCHIDEE}^{0.162,VISIT}$ m^2m^{-2} for JJA, and RMSD ranging from $0.036_{0.026,ORCHIDEE}^{0.109,VISIT}$ m^2m^{-2} for MAM to $0.043_{0.040,CABLE}^{0.135,VISIT}$ m^2m^{-2} for SON).

The traditional MME method reduced the uncertainties in model parameterization and structure to some extent, yet this method inherently treats all models equally regardless of their performance in reproducing the changes in observed seasonal mean LAI. In this study, we synthesized the 10 ecosystem models based on the BMA strategy, which explicitly evaluated the performance of individual models in simulating observed LAI changes, assigned weights for the models accordingly, and then attributed the contributions of the potential driving factors to seasonal LAI changes based on the optimized integration of the 10 ecosystem models. Fig. 4 shows the spatial pattern of models that were assigned the largest BMA weights and their total area fraction for each season. Generally, the performances of the ecosystem models in simulating LAI changes were region specific; i.e., one model may have performed better in one region, whereas other models may have performed better in another. During MAM, ORCHIDEE had the largest area and was assigned the maximum BMA weight (32.01%), mainly distributed in central North America and the mid-latitudes of Eurasia. CABLE exhibited the best performance in the northern latitudes of North America and ranked second place in terms of the area fraction of the maximum BMA weight (21.46%).

CABLE well captured seasonal LAI changes over the largest vegetated area fraction during JJA (24.09%) and SON (39.29%), followed by ORCHIDEE (JJA, 18.60%; SON, 21.66%).

Fig. 5 shows the comparison of spatial patterns between the seasonal LAI trends estimated from MME and those estimated from BMA. Generally, the BMA optimized model ensemble was significantly superior to the MME results in terms of reproducing the observed LAI trends during all seasons. The spatial pattern of trends in MME seasonal LAI partly captured the observed seasonal LAI trend pattern, although important differences were found, particularly during SON (Fig. 6 and S4). During MAM, trends in MME LAI over 43.9% of the vegetated area lay within the boundary of the trends for the three remotely sensed LAI values, which were mainly distributed in the mid–high latitudes (Fig. 6a). The MME underestimated LAI trends for 20.0% of the vegetated area, mainly located in the western United States, northern China, and eastern Mongolia, but overestimated LAI trends for 36.1% of the vegetated area, mainly distributed in the northern latitudes, central North America, and other small regions in Eurasia. In contrast, BMA reproduced well the observed trends over 66.36% of the vegetated area, and underestimated and overestimated observed LAI trends over 19.12 and 17.53% of the vegetated area, respectively. The main differences between observed LAI trends and BMA LAI trends were detected in southwestern North America and central Asia (Fig. 6b). The spatial pattern of the comparison between MME LAI trends and observed LAI trends during JJA was similar to that during MAM, except for notable underestimation in Europe (Fig. 6c). BMA LAI significantly reduced discrepancies between simulated LAI trends and observed LAI trends, although the BMA LAI still underestimated observed trends over a small area in Europe (Fig. 6d). During JJA, MME (BMA) LAI captured the observed LAI trends over 46.4% (66.07%) of the vegetated area, but underestimated and overestimated the LAI trends over 26.6% (21.41%) and 27.1% (12.52%), respectively. During SON, the MME simulation of observed LAI trends was conspicuously poor, capturing observed LAI trends over 29.4% of the vegetated area, while underestimating and overestimating LAI trends over 27.1% and 43.5% of the northern vegetated lands. Notable overestimation of the SON LAI trends occurred mainly over the high latitudes in North America and Eurasia (Fig. 6e). BMA LAI improved simulated LAI trends to some extent; the area fractions of good estimation, underestimation, and overestimation were 51.06, 24.37, and 24.57%, respectively (Fig. 6f). The main regions where BMA LAI trend underestimation occurred were southwestern North America and Europe, whereas the regions in which overestimation occurred were fragmentally distributed over Alaska, the central United States, northwestern Russia, central Asia, and southern China. The general consistency between BMA LAI and remotely sensed LAI imply that the ecosystem models combined with the Bayesian model averaging integration strategy are more appropriate for the analysis of potential drivers of LAI changes in the northern latitudes. Thus, the following attribution of seasonal LAI changes in the northern latitudes during 1982–2009 was based on the BMA integrated factorial simulations of the 10 ecosystem models.

At the hemispheric scale, LAI trends during all seasons simulated by ecosystem models with all factors considered were comparable to observed seasonal LAI trends (Fig. 7). Ecosystem models also captured the orders of magnitude of the observed seasonal LAI trends, i.e., JJA ($0.0066^{0.0211,VISIT}_{0.0029,ORCHIDEE}$ m^{2} m^{-2} yr^{-1}), SON ($0.0045^{0.0205,VISIT}_{0.0030,LPJ}$ m^{2} m^{-2} yr^{-1}), and MAM ($0.0030^{0.0161,VISIT}_{0.0013,LPJ}$ m^{2} m^{-2} yr^{-1}). During all seasons, increases in LAI due to increasing atmospheric CO_2 concentration explained the largest fraction of the observed greening trends in the northern latitudes (0.0019–0.0032 m^2 m^{-2} yr^{-1}), whereas climate change explained slightly less (0.0007–0.0024 m^2 m^{-2} yr^{-1}) (Fig. 7). Compared to eCO_2 and climate change, the effects of nitrogen deposition and land cover change explained only a small part of the observed seasonal LAI trends, around 0.0002 m^2 m^{-2} yr^{-1} and ranging from 0.0001 m^2 m^{-2} yr^{-1} to 0.0010 m^2 m^{-2} yr^{-1}, respectively. These driving factors generally provided the largest contributions to greening trends during JJA over the northern latitudes.

The spatial pattern of eCO_2 effects on seasonal LAI trends was uniformly distributed over the northern latitudes (Fig. 8). Conversely, the spatial pattern of climate change effects was heterogeneous and dominated the spatial variation in seasonal LAI trends (Fig. 8). Ecosystem models indicated that climate change had led to increases in seasonal LAI over 62.83% (MAM, 23.32%, $p < 0.05$) to 74.19% (JJA, 45.86%, $p < 0.05$) of the vegetated area, and had led to decreases in seasonal LAI over 25.70% (JJA, 7.52%, $p < 0.05$) to 37.13% (MAM, 8.31%, $p < 0.05$) of the vegetated area. The increasing LAI trends due to climate change were mainly distributed over southeastern North America, Western Europe, and Russia, probably due to warming (Fig. 9). The decreases in LAI trends due to climate change occurred in southwestern North America, Eastern Europe, and eastern Mongolia. Decreasing water availability was likely the dominant climate variable driving LAI decreases over these regions (Fig. 9 and S9).

Land cover change exhibited strong local effects on LAI trends, although these effects were relatively small at the hemispherical scale. Notable positive land cover change effects were mainly distributed over southeastern North America, Eastern Europe, and southeastern

China, likely due to agricultural activities, forest regrowth, and plantation in these regions. Negative land cover change effects were relatively small and generally distributed over regions where grazing is extensive (Kawamura *et al.*, 2005, Li *et al.*, 2016).

The effects of nitrogen deposition on vegetation were generally weak compared to other driving factors. Positive nitrogen deposition effects were simulated over a large fraction of the vegetated lands in the northern latitudes, consistent with increasing total nitrogen deposition rates in the northern hemisphere (Galloway *et al.*, 2008, LeBauer & Treseder, 2008, Liu *et al.*, 2013). However, we also observed significant negative trends in LAI due to changes in nitrogen deposition in Eastern Europe. This observation may be partly explained by the decreasing nitrogen deposition rate in these regions during recent decades due to reforestation and nitrogen purification of anthropogenic emissions (Baker & Samantha, 2009, Holland *et al.*, 2005).

During all seasons, the fraction of the vegetated area where climate change contributed most greatly to vegetation greening were larger (MAM, 38.96%; JJA, 46.06%; SON, 42.27%) than those of other potential driving factors (Fig. 10). This dominant climate change effect was more prominent in the high latitudes. For example, the dominant climate change effect was widely distributed across Russia and northeastern Canada (Fig. 10). The CO_2 fertilization effect dominated the second largest vegetated area showing greening trends during all seasons (MAM, 35.00%; JJA, 30.59%; SON, 32.57%); however, the spatial pattern of the dominant CO_2 fertilization effect was fragmented (Fig. 10). The spatial pattern of the dominant land use change effect was more clustered than that of the dominant CO_2 fertilization effect, and was mainly distributed over eastern North America, Europe, and northern China. The land use change effect dominated 9.79, 8.83, and 9.29% of the vegetated area during MAM, JJA, and SON, respectively. The fractions of vegetated area where nitrogen deposition was the dominant effect were small (<3%) during all seasons.

Discussion

Contributions of trends in maximum LAI and growing season length to annual LAI trends

Previous studies expressed the growing season productivity, which is well correlated with growing season mean LAI, as the product of maximum productivity and the length of the growing season (Xia *et al.*, 2015). This expression implicitly assumes that the roles of maximum productivity and the growing season length are equally important in determining the growing season productivity of plants. However, our study revealed that maximum productivity (LAI_{max}) trends dominate annual productivity (annual mean LAI) trends. LAI trends during JJA contributed 47.7% of the annual LAI trends over the northern latitudes, whereas the contributions of LAI trends during MAM and SON were much smaller (16.3 and 25.4%, respectively). The increases in LAI during MAM and SON were the consequence of longer growing days and enhanced photosynthetic capability. Environmental factors such as radiation and nutrient and water availability were at very low levels for photosynthesis during the extended growing days in early spring and late autumn. Although the spatial pattern of LAI trends during MAM/SON were well matched with the SOS/EOS trend pattern (Fig. S9), earlier SOS or delayed EOS were unlikely to lead to significant increases in productivity. A possible reason for similar patterns in MAM/SON LAI trends and SOS/EOS trends is that they are co-limited by identical environmental factors. For example, the start of the growing season in the northern latitudes is thought to be driven mainly by temperature increase, which also benefits photosynthesis by releasing temperature limitations on plant biological processes (Nemani *et al.*, 2003).

According to state-of-the-art ecosystem models, the asymmetric seasonal LAI response to increasing atmospheric CO_2 concentration is one explanation for our observation of a maximum increase in LAI during summer. The ecosystem models indicated that eCO_2 led to increasing LAI trends at a magnitude of 0.0032 m^2 m^{-2} yr^{-1} during summer, about 1.7 times the LAI trends during spring. Although the amplitude of the seasonal change in atmospheric CO_2 concentration in the northern latitudes has been increasing during recent decades(Forkel *et al.*, 2016, Graven *et al.*, 2013, Keeling *et al.*, 1996b), differences in the seasonal increases in atmospheric CO_2 concentration were not significant during 1982–2009 (MAM, 44.82 ppm; JJA, 44.78 ppm; SON, 45.15 ppm). Thus, the same increases in atmospheric CO_2 concentration have noticeably different effects on vegetation LAI in different seasons in the northern latitudes. The asymmetric seasonal eCO_2 fertilization effects on vegetation LAI are consistent with those on vegetation photosynthesis capacity from observation and theoretical expectations (Lewis *et al.*, 1996). Given the same increases in atmospheric CO_2

concentration, it appears that better hydrothermal conditions during summer allow vegetation to assimilate more carbohydrate that can be used to form more leaves.

Uncertainties in model-simulated and remotely sensed seasonal LAI trends

Our results yielded significant differences between remotely sensed seasonal LAI trends and MME seasonal LAI trends (Fig. S7), indicating large uncertainties within state-of-the-art ecosystem models and/or uncertainties in remotely sensed seasonal LAI trends (Anav *et al.*, 2013a, Anav *et al.*, 2013b, Zhu *et al.*, 2016). Uncertainties in ecosystem models are likely due to non-modeled ecosystem processes and poor representation of existing ecosystem processes and uncertainties in driving data sets (van den Hurk *et al.*, 2016, Wang *et al.*, 2011a). In some regions, the spatial distribution of croplands overlapped with areas showing significant residual seasonal LAI trends (e.g., southeastern North America, Western Europe, and eastern China), which is likely due to the fact that Agricultural activities are generally not well represented in current ecosystem models. For example, current ecosystem model still has many problems in representing intra-seasonal variations in LAI due to multiple cropping (Jeong *et al.*, 2014). Additionally, current ecosystem models tend to be oversensitive to water availability (Piao *et al.*, 2013), which appears to be a significant source of uncertainty in modeling vegetation LAI changes (Zhu *et al.*, 2016). The geolocations where significant seasonal increases in soil water content (SWC) occurred were generally associated with negative residual seasonal trends, i.e., the model overestimated seasonal LAI trends, whereas the regions where significant seasonal SWC decreased were associated with positive residual seasonal LAI trends, i.e., the model underestimated seasonal LAI trends. Wildfire, together with significant SWC decreases, appears to explain the significant negative residual seasonal LAI trends in Alaska. However, there remained regions where large differences between satellite observations and model simulations were found that cannot be explained by agricultural activities, water availability changes, or wildfire. For example, significant positive residuals were found in Eastern Europe during MAM, JJA, and SON; however, no potential uncertainty source was found. A possible explanation for the underestimation of ecosystem models is forest regrowth and afforestation during recent decades in that region, as occurred in southeastern North America (Pan *et al.*, 2011). Moreover, the phenology modules of the ecosystem models are thought to be not reliable, especially when complex mechanisms are incorporated (Murray-Tortarolo *et al.*, 2013). Our results show larger discrepancies between simulated LAI trends and remotely sensed LAI trends during autumn than during other seasons, which is consistent with a previous study suggesting a relatively large bias in simulated dormancy dates during the growing season by current ecosystem models (Murray-Tortarolo *et al.*, 2013). We suggest that improving the phenology module of current ecosystem models is a crucial first step toward improving our understanding of seasonal LAI changes.

Additionally, seasonal variation in nitrogen deposition rates and land cover change are generally not well represented in the current ecosystem models (Thomas *et al.*, 2013, Wang *et al.*, 2010, Zaehle *et al.*, 2010). For example, many ecosystem models evenly assign the annual nitrogen deposition amount to each day due to the limitations caused by the temporal resolution of the nitrogen deposition driving data set (Wang *et al.*, 2010). Similarly, the land cover change driving data sets used in the ecosystem models are typically updated annually. Uncertainties in the driving data sets tend to undermine the ability of the ecosystem models to simulate actual seasonal variation in the effects of nitrogen deposition and land use change on LAI trends. Thus, our study provides a simplified illustration of the contribution of nitrogen deposition and land use change to seasonal LAI trends.

Discrepancies in seasonal LAI trends between observed data and model simulations may also be due to uncertainties in the three remotely sensed LAI data sets. GIMMS LAI3g, GLASS LAI, and GLOBMAP LAI are three widely used long-term LAI products that provide global LAI records starting from the early 1980s. All of the LAI products have been extensively validated against field measurements and other satellite products, which supports their suitability for long-term vegetation research. However, we should also be mindful of their uncertainties. Although all three LAI products used in this study consistently showed the dominant greening trends over the northern latitudes, the spatial distribution and magnitudes of LAI trends were somewhat different (Fig. S3). There are several potential reasons for these discrepancies and uncertainties in the LAI products. First, the LAI products were generated using different strategies and different AVHRR products. Second, AVHRR sensors lack on-board calibration and have orbital loss problems, which cause biases that cannot easily be quantified. Third, although GLASS and GLOBMAP proposed their own methods to merge LAI derived from AVHRR sensors and MODIS, it is still difficult to create a consistent LAI time series because AVHRR and MODIS sensors have different spectral characteristics. These problems may be alleviated by generating accurate and consistent LAI time series data in the future.

In summary, we tentatively quantified seasonal LAI trends and the effects of eCO_2, climate change, nitrogen deposition, and land use change on seasonal LAI trends between 1982 and 2009 in the northern latitudes (north of 30°N) based on three remotely sensed long-term LAI data sets and 10 state-of-the-art ecosystem models. Although our immediate objectives have been achieved, there are several aspects that should be addressed in future studies. First, both remotely sensed LAI data sets and model-simulated LAI outputs showed large uncertainties. Further refinements of satellite observation and retrieval techniques and ecosystem models are the fundamental requirements for accurate detection and attribution of seasonal vegetation growth changes. Second, the attribution method used in this study assumed that the effects of the potential driving factors were additive and did not explicitly consider interactions among the driving factors (Zhang *et al.*, 2016). Additionally, the lag effects of some environmental factors across seasons were not taken into account. For example, warming and warming-induced greening during MAM should have led to increases in evapotranspiration during MAM (Huang *et al.*, 2016) and reduced soil water content during MAM (Wolf *et al.*, 2016), which would limit vegetation growth during JJA. Also, drought-induced tree mortality (Allen *et al.*, 2010, Dietze & Moorcroft, 2011, van Mantgem *et al.*, 2009) during JJA should strongly affect vegetation growth during SON and the subsequent seasons. Finally, although the factorial experiments based on the 10 ecosystem models made it possible to separate the effects of nitrogen deposition and land use change on trends in seasonal vegetation LAI, we should be aware of inherent deficiencies in the spatial and temporal resolution of input data for both nitrogen deposition and land use change, and in the representation of related biophysical processes. Applying high-quality spatiotemporal nitrogen deposition and land use change data and incorporating and improving processes related to phenology, agricultural activities and wildfires should be priorities for the refinement of current ecosystem models.

Acknowledgements

This study was supported by the National Basic Research Program of China (Grant No. 2013CB956303), the National Natural Science Foundation of China (41561134016), and National Youth Top-notch Talent Support Program in China. We thank the TRENDY modelling group for providing the TRENDYv2 model data.

References

Ajami NK, Duan Q, Sorooshian S (2007) An Integrated Hydrologic Bayesian Multimodel Combination Framework: Confronting Input, Parameter, and Model Structural Uncertainty in Hydrologic Prediction. Water Resources Research, **43**, W01403.

Allen CD, Macalady AK, Chenchouni H *et al.* (2010) A Global Overview of Drought and Heat-Induced Tree Mortality Reveals Emerging Climate Change Risks for Forests. Forest Ecology and Management, **259**, 660-684.

Anav A, Friedlingstein P, Kidston M *et al.* (2013a) Evaluating the Land and Ocean Components of the Global Carbon Cycle in the CMIP5 Earth System Models. Journal of Climate, **26**, 6801-6843.

Anav A, Murray-Tortarolo G, Friedlingstein P, Sitch S, Piao S, Zhu Z (2013b) Evaluation of Land Surface Models in Reproducing Satellite Derived Leaf Area Index over the

High-Latitude Northern Hemisphere. Part Ii: Earth System Models. Remote Sensing, **5**, 3637.

Anderegg WRL, Hicke JA, Fisher RA *et al.* (2015) Tree Mortality from Drought, Insects, and Their Interactions in a Changing Climate. New Phytologist, **208**, 674-683.

Baker, Samantha MH (2009) *Atmospheric Ammonia : Detecting Emission Changes and Environmental Impacts : Results of an Expert Workshop under the Convention on Long-Range Transboundary Air Pollution*, Springer.

Bellucci A, Haarsma R, Bellouin N *et al.* (2015) Advancements in Decadal Climate Predictability: The Role of Nonoceanic Drivers. Reviews of Geophysics, **53**, 165-202.

Chaves MM, Pereira JS, Maroco J *et al.* (2002) How Plants Cope with Water Stress in the Field? Photosynthesis and Growth. Annals of Botany, **89**, 907-916.

Cohen JL, Furtado JC, Barlow M, Alexeev VA, Cherry JE (2012) Asymmetric Seasonal Temperature Trends. Geophysical Research Letters, **39**, L04705.

Dardel C, Kergoat L, Hiernaux P, Mougin E, Grippa M, Tucker CJ (2014) Re-Greening Sahel: 30 Years of Remote Sensing Data and Field Observations (Mali, Niger). Remote Sensing of Environment, **140**, 350-364.

Dietze MC, Moorcroft PR (2011) Tree Mortality in the Eastern and Central United States: Patterns and Drivers. Global Change Biology, **17**, 3312-3326.

Donohue RJ, Roderick ML, Mcvicar TR, Farquhar GD (2013) Impact of CO_2 Fertilization on Maximum Foliage Cover across the Globe's Warm, Arid Environments. Geophysical Research Letters, **40**, 3031-3035.

Flato G, Marotzke J, Abiodun B *et al.* (2013) Evaluation of Climate Models. In: *Climate Change 2013: The Physical Science Basis. Contribution of Working Group I to the Fifth Assessment Report of the Intergovernmental Panel on Climate Change.* (eds Stocker TF, Qin D, Plattner G-K, Tignor M, Allen SK, Boschung J, Nauels A, Xia Y, Bex V, Midgley PM) pp Page. Cambridge, United Kingdom and New York, NY, USA, Cambridge University Press.

Forkel M, Carvalhais N, Rödenbeck C *et al.* (2016) Enhanced Seasonal CO_2 Exchange Caused by Amplified Plant Productivity in Northern Ecosystems. Science, **351**, 696-699.

Furrer R, Knutti R, Sain SR, Nychka DW, Meehl GA (2007) Spatial Patterns of Probabilistic Temperature Change Projections from a Multivariate Bayesian Analysis. Geophysical Research Letters, **34**, L06711.

Galloway JN, Townsend AR, Erisman JW *et al.* (2008) Transformation of the Nitrogen Cycle: Recent Trends, Questions, and Potential Solutions. Science, **320**, 889-892.

Giorgi F, Mearns LO (2002) Calculation of Average, Uncertainty Range, and Reliability of Regional Climate Changes from Aogcm Simulations Via the "Reliability Ensemble Averaging" (Rea) Method. Journal of Climate, **15**, 1141-1158.

Graven HD, Keeling RF, Piper SC *et al.* (2013) Enhanced Seasonal Exchange of CO_2 by Northern Ecosystems since 1960. Science, **341**, 1085-1089.

Greaver TL, Clark CM, Compton JE *et al.* (2016) Key Ecological Responses to Nitrogen Are Altered by Climate Change. Nature Clim. Change, **6**, 836-843.

Hember RA, Kurz WA, Coops NC (2017) Relationships between Individual-Tree Mortality and Water-Balance Variables Indicate Positive Trends in Water Stress-Induced Tree Mortality across North America. Global Change Biology, **23**, 1691-1710.

Hoeting JA, Madigan D, Raftery AE, Volinsky CT (1999) Bayesian Model Averaging: A Tutorial. Statistical Science, **14**, 382-401.

Holland EA, Braswell BH, Sulzman J, Lamarque JF (2005) Nitrogen Deposition onto the United States and Western Europe: Synthesis of Observations and Models. Ecological Applications, **15**, 38-57.

Huang M, Piao S, Zeng Z *et al.* (2016) Seasonal Responses of Terrestrial Ecosystem Water-Use Efficiency to Climate Change. Global Change Biology, **22**, 2165-2177.

Huang MT, Piao SL, Sun Y *et al.* (2015) Change in Terrestrial Ecosystem Water-Use Efficiency over the Last Three Decades. Global Change Biology, **21**, 2366-2378.

IPCC (2013) *Climate Change 2013: The Physical Science Basis. Contribution of Working Group I to the Fifth Assessment Report of the Intergovernmental Panel on Climate Change,* Cambridge, United Kingdom and New York, NY, USA, Cambridge University Press.

Jeong S-J, Ho C-H, Gim H-J, Brown ME (2011) Phenology Shifts at Start Vs. End of Growing Season in Temperate Vegetation over the Northern Hemisphere for the Period 1982–2008. Global Change Biology, **17**, 2385-2399.

Jeong S-J, Ho C-H, Piao S *et al.* (2014) Effects of Double Cropping on Summer Climate of the North China Plain and Neighbouring Regions. Nature Clim. Change, **4**, 615-619.

Kawamura K, Akiyama T, Yokota H-O, Tsutsumi M, Yasuda T, Watanabe O, Wang S (2005) Quantifying Grazing Intensities Using Geographic Information Systems and Satellite Remote Sensing in the Xilingol Steppe Region, Inner Mongolia, China. Agriculture, Ecosystems & Environment, **107**, 83-93.

Keeling CD, Chin JFS, Whorf TP (1996a) Increased Activity of Northern Vegetation Inferred from Atmospheric CO_2 Measurements. Nature, **382**, 146-149.

Keeling CD, Whorf TP (2005) Atmospheric CO_2 Records from Sites in the Sio Air Sampling Network. Trends: a compendium of data on global change, **2009**.

Keeling RF, Piper SC, Heimann M (1996b) Global and Hemispheric CO_2 Sinks Deduced from Changes in Atmospheric O_2 Concentration. Nature, **381**, 218-221.

Lawrence DM, Oleson KW, Flanner MG *et al.* (2011) Parameterization Improvements and Functional and Structural Advances in Version 4 of the Community Land Model. Journal of Advances in Modeling Earth Systems, **3**, M03001.

Le Quéré C, Moriarty R, Andrew RM *et al.* (2015) Global Carbon Budget 2015. Earth Syst. Sci. Data*,* **7**, 349-396.

Le Quéré C, Peters GP, Andres RJ *et al.* (2013) Global Carbon Budget 2013. Earth Syst. Sci. Data Discuss.*,* **6**, 689-760.

Lebauer DS, Treseder KK (2008) Nitrogen Limitation of Net Primary Productivity in Terrestrial Ecosystems Is Globally Distributed. Ecology*,* **89**, 371-379.

Lewis JD, Tissue DT, Strain BR (1996) Seasonal Response of Photosynthesis to Elevated CO_2 in Loblolly Pine (Pinus Taeda L.) over Two Growing Seasons. Global Change Biology*,* **2**, 103-114.

Li F, Zheng J, Wang H, Luo J, Zhao Y, Zhao R (2016) Mapping Grazing Intensity Using Remote Sensing in the Xilingol Steppe Region, Inner Mongolia, China. Remote Sensing Letters*,* **7**, 328-337.

Liu Q, Fu YH, Zhu Z *et al.* (2016) Delayed Autumn Phenology in the Northern Hemisphere Is Related to Change in Both Climate and Spring Phenology. Global Change Biology*,* **22**, 3702-3711.

Liu X, Zhang Y, Han W *et al.* (2013) Enhanced Nitrogen Deposition over China. Nature*,* **494**, 459-462.

Liu Y, Liu RG, Chen JM (2012) Retrospective Retrieval of Long-Term Consistent Global Leaf Area Index (1981-2011) from Combined AVHRR and MODIS Data. Journal of Geophysical Research-Biogeosciences*,* **117**, G04003.

Los SO (2013) Analysis of Trends in Fused AVHRR and MODIS NDVI Data for 1982-2006: Indication for a CO_2 Fertilization Effect in Global Vegetation. Global Biogeochemical Cycles*,* **27**, 318-330.

Lucht W, Prentice IC, Myneni RB *et al.* (2002) Climatic Control of the High-Latitude Vegetation Greening Trend and Pinatubo Effect. Science*,* **296**, 1687-1689.

Mao J, Ribes A, Yan B *et al.* (2016) Human-Induced Greening of the Northern Extratropical Land Surface. Nature Clim. Change, **6**, 959-963.

Mao J, Shi X, Thornton PE, Hoffman FM, Zhu Z, Myneni RB (2013) Global Latitudinal-Asymmetric Vegetation Growth Trends and Their Driving Mechanisms: 1982-2009. Remote Sensing, **5**, 1484-1497.

Martre P, Wallach D, Asseng S *et al.* (2015) Multimodel Ensembles of Wheat Growth: Many Models Are Better Than One. Global Change Biology, **21**, 911-925.

Medlyn BE, Dreyer E, Ellsworth D *et al.* (2002) Temperature Response of Parameters of a Biochemically Based Model of Photosynthesis. Ii. A Review of Experimental Data. Plant, Cell & Environment, **25**, 1167-1179.

Milliff RF, Bonazzi A, Wikle CK, Pinardi N, Berliner LM (2011) Ocean Ensemble Forecasting. Part I: Ensemble Mediterranean Winds from a Bayesian Hierarchical Model. Quarterly Journal of the Royal Meteorological Society, **137**, 858-878.

Murray-Tortarolo G, Anav A, Friedlingstein P *et al.* (2013) Evaluation of Land Surface Models in Reproducing Satellite-Derived LAI over the High-Latitude Northern Hemisphere. Part I: Uncoupled Dgvms. Remote Sensing, **5**, 4819.

Myneni RB, Keeling CD, Tucker CJ, Asrar G, Nemani RR (1997) Increased Plant Growth in the Northern High Latitudes from 1981 to 1991. Nature, **386**, 698-702.

Nemani RR, Keeling CD, Hashimoto H *et al.* (2003) Climate-Driven Increases in Global Terrestrial Net Primary Production from 1982 to 1999. Science, **300**, 1560-1563.

Neuman SP (2003) Maximum Likelihood Bayesian Averaging of Uncertain Model Predictions. Stochastic Environmental Research and Risk Assessment, **17**, 291-305.

New M, Hulme M, Jones P (2000) Representing Twentieth-Century Space-Time Climate Variability. Part Ii: Development of 1901-96 Monthly Grids of Terrestrial Surface Climate. Journal of Climate, **13**, 2217-2238.

Pan Y, Birdsey RA, Fang J *et al.* (2011) A Large and Persistent Carbon Sink in the World's Forests. Science, **333**, 988-993.

Piao S, Friedlingstein P, Ciais P, Viovy N, Demarty J (2007) Growing Season Extension and Its Impact on Terrestrial Carbon Cycle in the Northern Hemisphere over the Past 2 Decades. Global Biogeochemical Cycles, **21**, GB3018.

Piao S, Friedlingstein P, Ciais P, Zhou L, Chen A (2006a) Effect of Climate and CO_2 Changes on the Greening of the Northern Hemisphere over the Past Two Decades. Geophysical Research Letters, **33**, L23402.

Piao S, Wang X, Ciais P, Zhu B, Wang TaO, Liu JIE (2011) Changes in Satellite-Derived Vegetation Growth Trend in Temperate and Boreal Eurasia from 1982 to 2006. Global Change Biology, **17**, 3228-3239.

Piao S, Yin G, Tan J *et al.* (2015) Detection and Attribution of Vegetation Greening Trend in China over the Last 30 years. Global Change Biology, **21**, 1601-1609.

Piao S, Fang J, He J (2006b) Variations in Vegetation Net Primary Production in the Qinghai-Xizang Plateau, China, from 1982 to 1999. Climatic Change, **74**, 253-267.

Piao S, Sitch S, Ciais P *et al.* (2013) Evaluation of Terrestrial Carbon Cycle Models for Their Response to Climate Variability and to CO_2 Trends. Global Change Biology, **19**, 2117-2132.

Raftery AE, Gneiting T, Balabdaoui F, Polakowski M (2005) Using Bayesian Model Averaging to Calibrate Forecast Ensembles. Monthly Weather Review, **133**, 1155-1174.

Reich PB, Hobbie SE, Lee TD (2014) Plant Growth Enhancement by Elevated CO_2 Eliminated by Joint Water and Nitrogen Limitation. Nature Geosci, **7**, 920-924.

Shen M, Piao S, Jeong S-J *et al.* (2015) Evaporative Cooling over the Tibetan Plateau Induced by Vegetation Growth. Proceedings of the National Academy of Sciences, **112**, 9299-9304.

Sitch S, Friedlingstein P, Gruber N *et al.* (2015) Recent Trends and Drivers of Regional Sources and Sinks of Carbon Dioxide. Biogeosciences, **12**, 653-679.

Sitch S, Smith B, Prentice IC *et al.* (2003) Evaluation of Ecosystem Dynamics, Plant Geography and Terrestrial Carbon Cycling in the LPJ Dynamic Global Vegetation Model. Global Change Biology, **9**, 161-185.

Taylor KE (2001) Summarizing Multiple Aspects of Model Performance in a Single Diagram. Journal of Geophysical Research-Atmospheres, **106**, 7183-7192.

Tebaldi C, Knutti R (2007) The Use of the Multi-Model Ensemble in Probabilistic Climate Projections. Philosophical Transactions of the Royal Society A: Mathematical, Physical and Engineering Sciences, **365**, 2053-2075.

Thomas RQ, Zaehle S, Templer PH, Goodale CL (2013) Global Patterns of Nitrogen Limitation: Confronting Two Global Biogeochemical Models with Observations. Global Change Biology, **19**, 2986-2998.

Tucker CJ, Pinzon JE, Brown ME *et al.* (2005) An Extended AVHRR 8-Km NDVI Dataset Compatible with MODIS and SPOT Vegetation NDVI Data. International Journal of Remote Sensing, **26**, 4485-4498.

Van Den Hurk B, Kim HJ, Krinner G *et al.* (2016) LS3MIP (V1.0) Contribution to CMIP6: The Land Surface, Snow and Soil Moisture Model Intercomparison Project - Aims, Setup and Expected Outcome. Geoscientific Model Development, **9**, 2809-2832.

Van Der Sleen P, Groenendijk P, Vlam M *et al.* (2015) No Growth Stimulation of Tropical Trees by 150 Years of CO_2 Fertilization but Water-Use Efficiency Increased. Nature Geosci, **8**, 24-28.

Van Mantgem PJ, Stephenson NL, Byrne JC *et al.* (2009) Widespread Increase of Tree Mortality Rates in the Western United States. Science, **323**, 521-524.

Vrugt J, Diks C, Clark M (2008) Ensemble Bayesian Model Averaging Using Markov Chain Monte Carlo Sampling. Environmental Fluid Mechanics, **8**, 579-595.

Wang W, Dungan J, Hashimoto H, Michaelis AR, Milesi C, Ichii K, Nemani RR (2011a) Diagnosing and Assessing Uncertainties of Terrestrial Ecosystem Models in a Multimodel Ensemble Experiment: 1. Primary Production. Global Change Biology, **17**, 1350-1366.

Wang X, Piao S, Ciais P, Li J, Friedlingstein P, Koven C, Chen A (2011b) Spring Temperature Change and Its Implication in the Change of Vegetation Growth in North America from 1982 to 2006. Proceedings of the National Academy of Sciences of the United States of America, **108**, 1240-1245.

Wang Y, Law RM, Pak B (2010) A Global Model of Carbon, Nitrogen and Phosphorus Cycles for the Terrestrial Biosphere. Biogeosciences, **7**, 2261-2282.

Wolf S, Keenan TF, Fisher JB *et al.* (2016) Warm Spring Reduced Carbon Cycle Impact of the 2012 Us Summer Drought. Proceedings of the National Academy of Sciences, **113**, 5880-5885.

Wu D, Zhao X, Liang S, Zhou T, Huang K, Tang B, Zhao W (2015) Time-Lag Effects of Global Vegetation Responses to Climate Change. Global Change Biology, **21**, 3520-3531.

Wu J, Albert LP, Lopes AP *et al.* (2016) Leaf Development and Demography Explain Photosynthetic Seasonality in Amazon Evergreen Forests. Science, **351**, 972-976.

Xia J, Niu S, Ciais P *et al.* (2015) Joint Control of Terrestrial Gross Primary Productivity by Plant Phenology and Physiology. Proceedings of the National Academy of Sciences, **112**, 2788-2793.

Xiao Z, Liang S, Wang J, Chen P, Yin X, Zhang LQ, Song J (2014) Use of General Regression Neural Networks for Generating the Glass Leaf Area Index Product from Time-Series Modis Surface Reflectance. Ieee Transactions on Geoscience and Remote Sensing, **52**, 209-223.

Xu L, Myneni RB, Chapin Iii FS *et al.* (2013) Temperature and Vegetation Seasonality Diminishment over Northern Lands. Nature Clim. Change*,* **3**, 581-586.

Yan H, Yu Q, Zhu Z-C, Myneni RB, Yan H-M, Wang S-Q, Shugart HH (2013) Diagnostic Analysis of Interannual Variation of Global Land Evapotranspiration over 1982–2011: Assessing the Impact of Enso. Journal of Geophysical Research: Atmospheres*,* **118**, 8969-8983.

Zaehle S, Friend AD, Friedlingstein P, Dentener F, Peylin P, Schulz M (2010) Carbon and Nitrogen Cycle Dynamics in the O-Cn Land Surface Model: 2. Role of the Nitrogen Cycle in the Historical Terrestrial Carbon Balance. Global Biogeochemical Cycles*,* **24**, GB1006.

Zeng N, Neelin JD, Chou C (2000) A Quasi-Equilibrium Tropical Circulation Model - Implementation and Simulation. Journal of the Atmospheric Sciences*,* **57**, 1767-1796.

Zhang X, Rayner PJ, Wang Y-P, Silver JD, Lu X, Pak B, Zheng X (2016) Linear and Nonlinear Effects of Dominant Drivers on the Trends in Global and Regional Land Carbon Uptake: 1959 to 2013. Geophysical Research Letters*,* **43**, 1607-1614.

Zhou L, Tucker CJ, Kaufmann RK, Slayback D, Shabanov NV, Myneni RB (2001) Variations in Northern Vegetation Activity Inferred from Satellite Data of Vegetation Index During 1981 to 1999. Journal of Geophysical Research-Atmospheres*,* **106**, 20069-20083.

Zhu Z, Piao S, Myneni RB *et al.* (2016) Greening of the Earth and Its Drivers. Nature Clim. Change*,* **6**, 791-795.

Zhu Z, Bi J, Pan Y *et al.* (2013) Global Data Sets of Vegetation Leaf Area Index (LAI)3g and Fraction of Photosynthetically Active Radiation (FPAR)3g Derived from Global Inventory Modeling and Mapping Studies (GIMMS) Normalized Difference Vegetation Index (NDVI3g) for the Period 1981 to 2011. Remote Sensing*,* **5**, 927-948.

Figure Captions

Figure 1. Trends in seasonal and monthly leaf area index (LAI) in northern latitudes during 1982–2009. (a) Overall trends in seasonal and monthly LAI in northern latitudes. Black line indicates trends in monthly LAI. (b) Spatial pattern of the trends in seasonal mean LAI for (b) spring (MAM), (c) summer (JJA), and (d) autumn (SON) based on the average of the three remotely sensed LAI data sets (GIMMS LAI3g, GLASS LAI, and GLOBMAP LAI). Trends in seasonal mean LAI for each pixel were estimated by linear regression. Black dots indicate that the trends are statistically significant ($p < 0.05$).

Figure 2. Dominant seasons of greening and browning in northern latitudes. (a) Spatial pattern of the dominant seasons of greening and browning. (b) Area fractions of the dominant seasons. The dominant season of a vegetated pixel is defined as the season that shows the maximum greening trend if the annual leaf area index (LAI) trend of the pixel is increasing, or the maximum browning trend if the annual LAI trend of the pixel is decreasing. Black horizontal lines indicate regions showing decreasing annual LAI trends.

Figure 3. Taylor diagrams (Taylor, 2001) compare the remotely sensed and model simulated seasonal leaf area index (LAI) in the northern latitudes for (a) spring (MAM), (b) summer (JJA) and (c) autumn (SON). The standard deviation shows the interannual variability of the observed and the modeled seasonal LAI. The dash green lines show centered root mean square difference (RMSD) between model simulations and satellite observation.

Figure 4. Spatial distribution of the maximum optimal weights of the 10 ecosystem models estimated by Bayesian model averaging (BMA) for (a) spring (MAM), (c) summer (JJA), and (e) autumn (SON), and the area fractions of the models assigned the maximum weights for (b) spring (MAM), (d) summer (JJA), and (f) autumn (SON) during 1982–2009.

Figure 5. Spatial pattern of the trends in model-simulated seasonal mean leaf area index (LAI) for (a) spring (MAM), (c) summer (JJA), and (e) autumn (SON) based on the multi-model ensemble (MME) mean method and for (b) spring (MAM), (d) summer (JJA), and (f) autumn (SON) based on Bayesian model averaging (BMA) during 1982–2009. Trends in seasonal mean LAI for each pixel were estimated by linear regression. Black dots indicate that the trends are statistically significant ($p < 0.05$).

Figure 6. Comparison of model performance in estimating trends in model-simulated seasonal monthly mean leaf area index (LAI) based on multi-model ensemble (MME) mean and Bayesian model averaging (BMA) during 1982–2009. Spatial pattern of performance of model-simulated seasonal mean LAI trends for (a) spring (MAM), (c) summer (JJA), and (e) autumn (SON) based on MME mean method and for (b) spring (MAM), (d) summer (JJA), and (f) autumn (SON) based on BMA. Model-simulated seasonal monthly mean LAI trends were compared to trends estimated from the three remotely sensed LAI data sets (GLASS LAI, GIMMS LAI and GLOBMAP LAI) to determine whether the model-simulated trend was within the range indicated by the remotely sensed data (Good), smaller than the

minimum trend of the remotely sensed data (Underestimate), or larger than the maximum trend of the remotely sensed data (Overestimate).

Figure 7. The observed (OBS), multi-model ensemble mean (MME) and Beyasian model averaging (BMA) trends in seasonal leaf area index (LAI) and the effects of atmospheric CO_2 concentration (CO_2), climate change (CLI), nitrogen deposition (NDE), and land use change (LCC) on seasonal LAI trends in the northern latitudes (north of 30°N) during 1982–2009. The effects of eCO_2, climate change, nitrogen deposition, and land use change were estimated from simulations S1, S2 – S1, S3 – S2, and S4 – S2 by the 10 ecosystem models. The 10 ecosystem models were integrated based on the Bayesian model averaging (BMA) method. The size of each sphere indicates the standard deviation of the seasonal LAI trends.

Figure 8. Spatial patterns of the effects of atmospheric CO_2 concentration (eCO_2), climate change, nitrogen deposition, and land use change on trends in seasonal leaf area index (LAI) in the northern latitudes (north of 30°N) during 1982–2009. The effects of eCO_2, climate change, nitrogen deposition, and land use change were estimated from simulations S1, S2 – S1, S3 – S2, and S4 – S2 by the 10 ecosystem models. The 10 ecosystem models were integrated based on the Bayesian model averaging (BMA) method. The seasonal monthly mean LAI trends were estimated by linear regression and tested with Student’s t-test. Black dots indicate that the trends are statistically significant ($p < 0.05$).

Figure 9. Spatial patterns of the effects of individual climatic variables (temperature, precipitation, and radiation) on trends in seasonal leaf area index (LAI) based on ORCHIDEE simulations in the northern latitudes during 1982–2009. Seasonal LAI trends were estimated by linear regression and tested with Student's t-test. Black dots indicate that the trends are statistically significant ($p < 0.05$). The pixel-wise spatial correlation coefficients between climate change effects on MAM, JJA and SON LAI trends simulated by ORCHIDEE and BMA model ensemble are 0.24 ($p<0.01$), 0.32 ($p<0.01$) and 0.14 ($p<0.01$), respectively.

Figure 10. Spatial pattern of the composition of the effects of driving factors (eCO_2, climate change, nitrogen deposition, and changes in land use and land cover) on seasonal leaf area index (LAI) during 1982–2009 for (a) March–May (MAM), (c) June–August (JJA), and (e) September–November (SON) and corresponding maps showing the sign of the effects of the driving factors for (b) MAM, (d) JJA), and (f) autumn (SON). Positive effects of eCO_2, climate change, and nitrogen deposition and land use/land cover change are abbreviated as O, C, and L, respectively. Thus, their compositions are abbreviated as CL, OL, OC, and OCL.

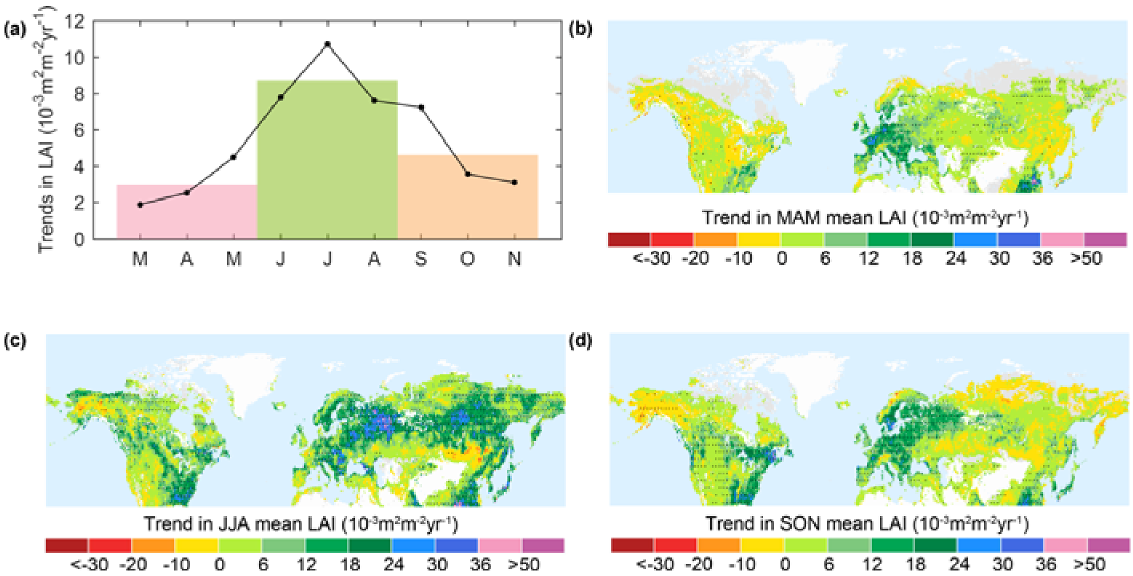
(a)
Trends in LAI (10^{-3}m^{2}m^{-2}yr^{-1})
12
10
8
6
4
2
0
M A M J J A S O N
(b)
Trend in MAM mean LAI (10^{-3}m^{2}m^{-2}yr^{-1})
<-30 -20 -10 0 6 12 18 24 30 36 >50
(c)
Trend in JJA mean LAI (10^{-3}m^{2}m^{-2}yr^{-1})
<-30 -20 -10 0 6 12 18 24 30 36 >50
(d)
Trend in SON mean LAI (10^{-3}m^{2}m^{-2}yr^{-1})
<-30 -20 -10 0 6 12 18 24 30 36 >50

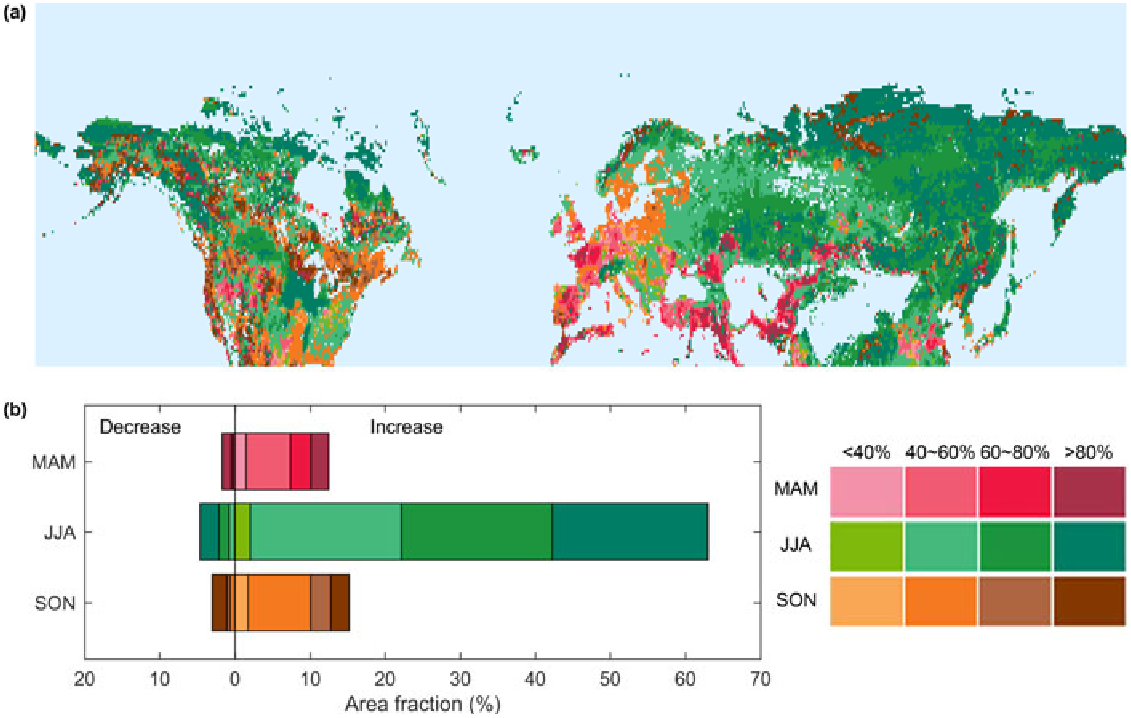
(a)
(b)
Decrease
Increase
MAM
JJA
SON
20 10 0 10 20 30 40 50 60 70
Area fraction (%)
<40% 40~60% 60~80% >80%
MAM
JJA
SON

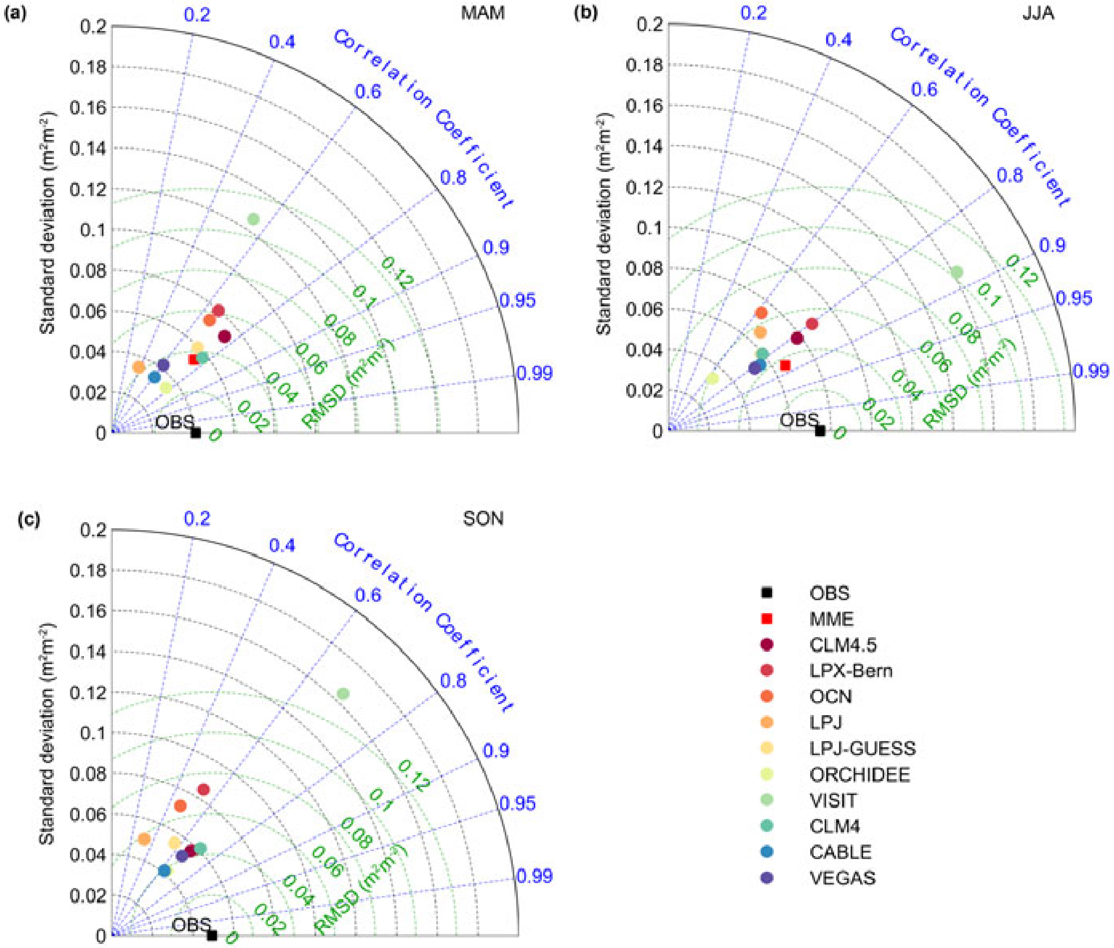
(a)
MAM
(b)
JJA
(c)
SON
Standard deviation (m^{2}m^{-2})
0
0.02
0.04
0.06
0.08
0.1
0.12
0.14
0.16
0.18
0.2
Correlation Coefficient
0.2
0.4
0.6
0.8
0.9
0.95
0.99
RMSD (m^{2}m^{-2})
0
0.02
0.04
0.06
0.08
0.1
0.12
OBS
■ OBS
■ MME
● CLM4.5
● LPX-Bern
● OCN
● LPJ
● LPJ-GUESS
● ORCHIDEE
● VISIT
● CLM4
● CABLE
● VEGAS

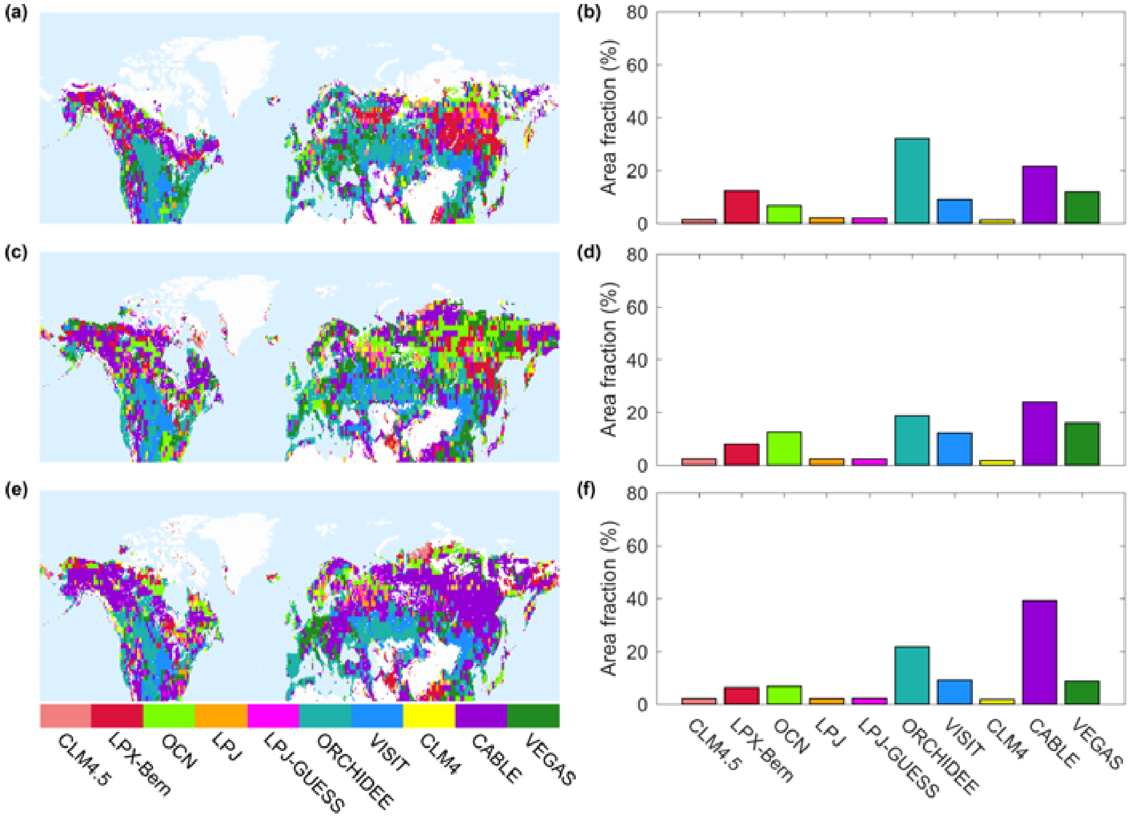
(a)
(b)
(c)
(d)
(e)
(f)
Area fraction (%)
0
20
40
60
80
CLM4.5
LPX-Bern
OCN
LPJ
LPJ-GUESS
ORCHIDEE
VISIT
CLM4
CABLE
VEGAS

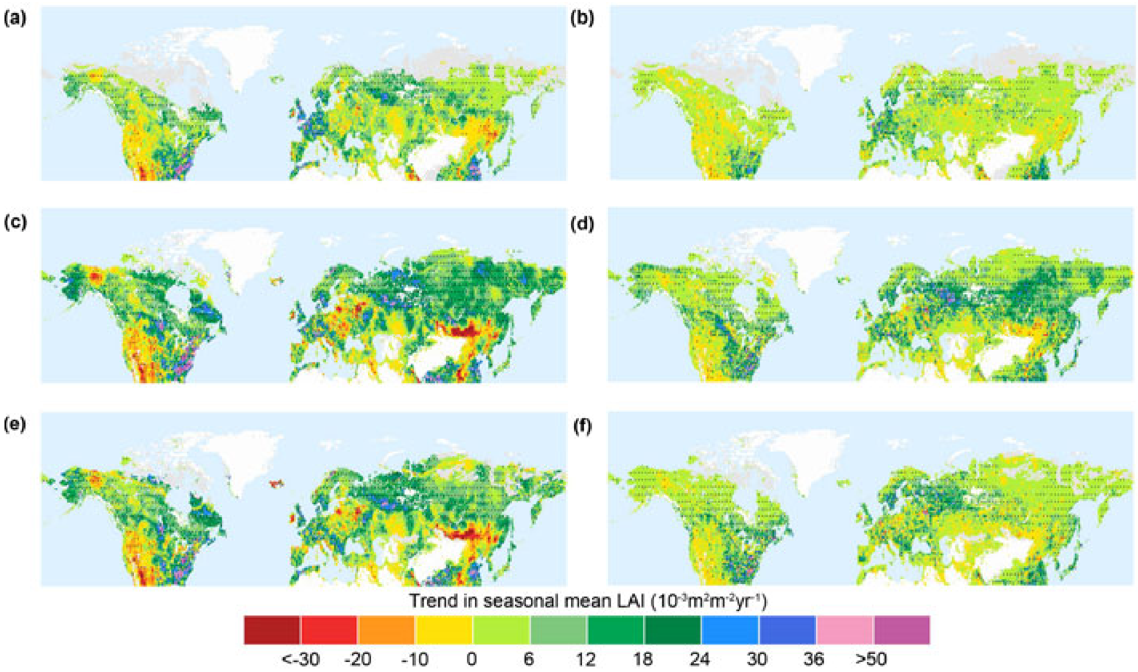
(a)
(b)
(c)
(d)
(e)
(f)
Trend in seasonal mean LAI ($10^{-3}m^2m^{-2}yr^{-1}$)
<-30
-20
-10
0
6
12
18
24
30
36
>50

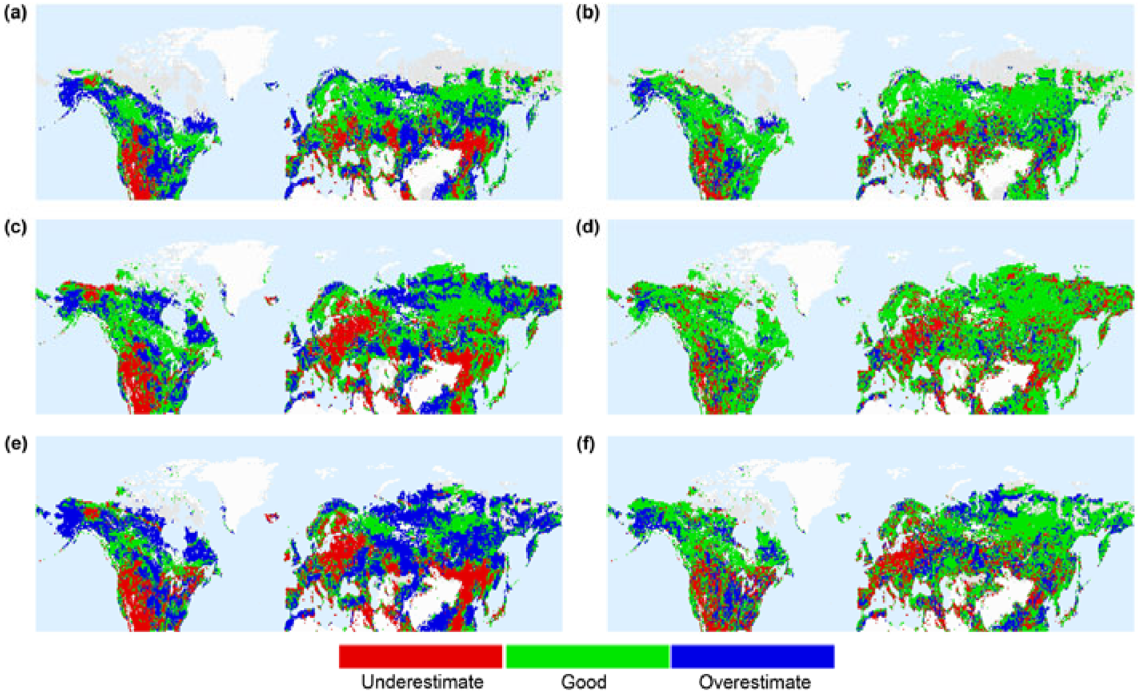
(a)
(b)
(c)
(d)
(e)
(f)
Underestimate
Good
Overestimate

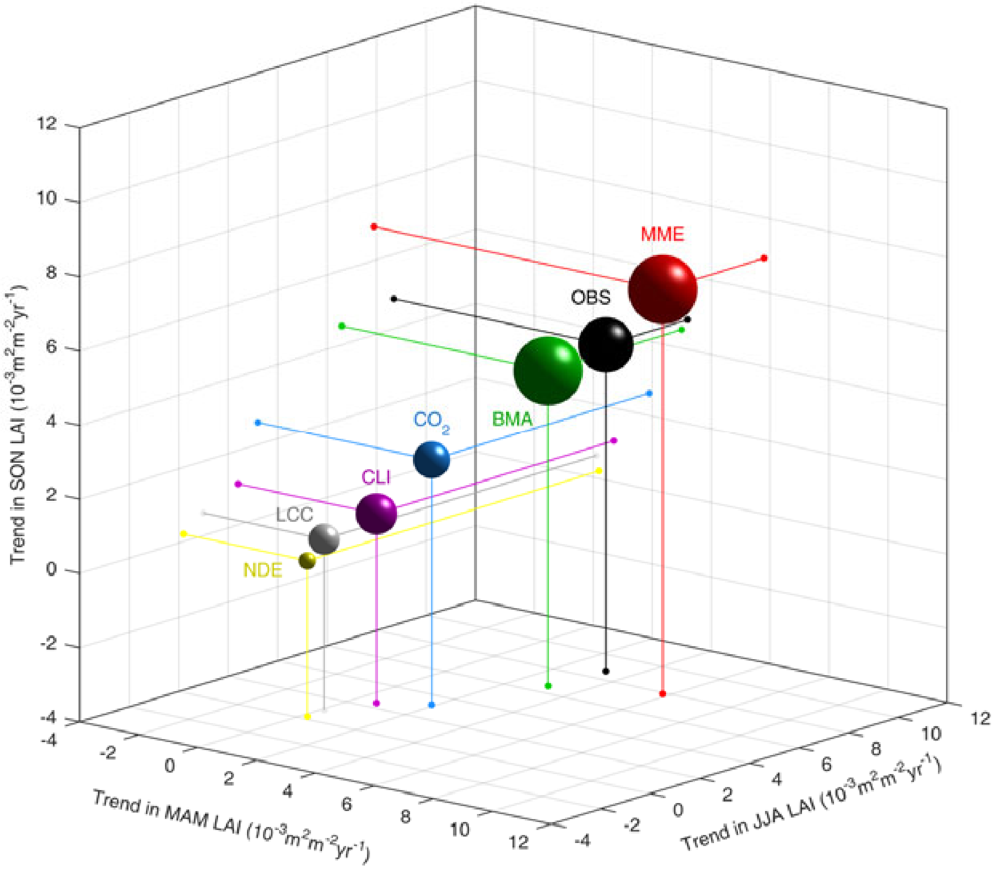
MME
OBS
BMA
CO$_2$
CLI
LCC
NDE
Trend in SON LAI ($10^{-3}m^2m^{-2}yr^{-1}$)
12
10
8
6
4
2
0
-2
-4
Trend in MAM LAI ($10^{-3}m^2m^{-2}yr^{-1}$)
-4
-2
0
2
4
6
8
10
12
Trend in JJA LAI ($10^{-3}m^2m^{-2}yr^{-1}$)
-4
-2
0
2
4
6
8
10
12

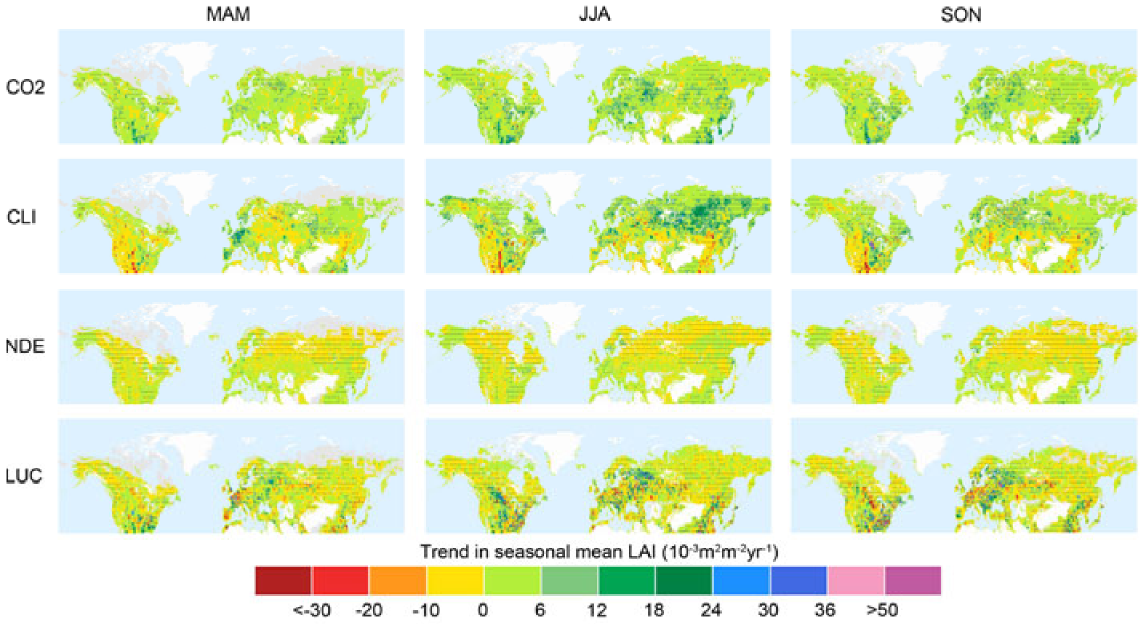
MAM
JJA
SON
CO2
CLI
NDE
LUC
Trend in seasonal mean LAI (10^{-3}m^{2}m^{-2}yr^{-1})
<-30
-20
-10
0
6
12
18
24
30
36
>50

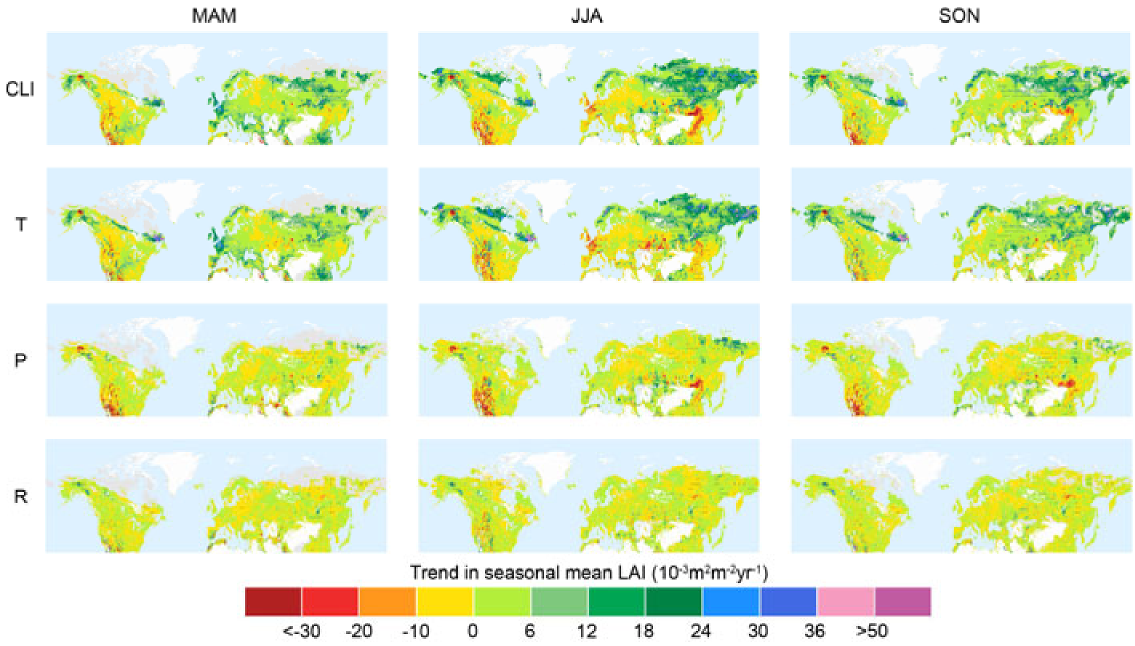
MAM
JJA
SON
CLI
T
P
R
Trend in seasonal mean LAI (10^{-3}m^{2}m^{-2}yr^{-1})
<-30
-20
-10
0
6
12
18
24
30
36
>50

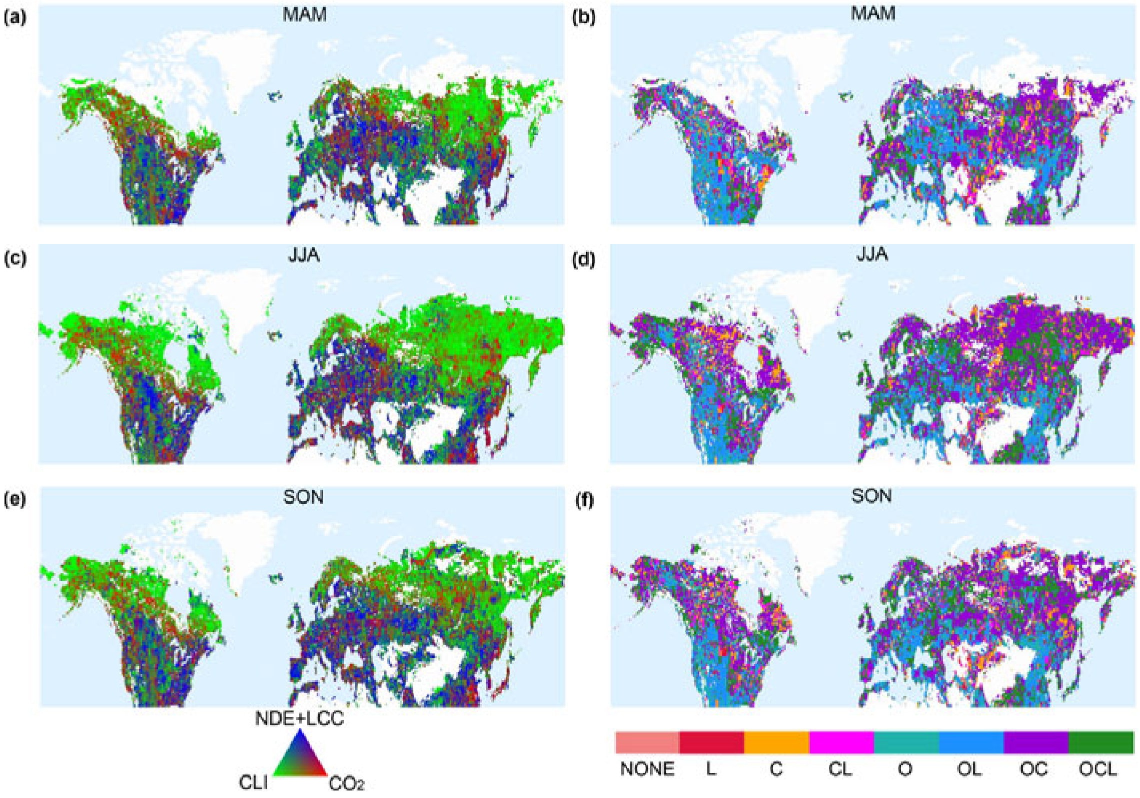
(a)
MAM
(b)
MAM
(c)
JJA
(d)
JJA
(e)
SON
(f)
SON
NDE+LCC
CLI
CO2
NONE
L
C
CL
O
OL
OC
OCL